

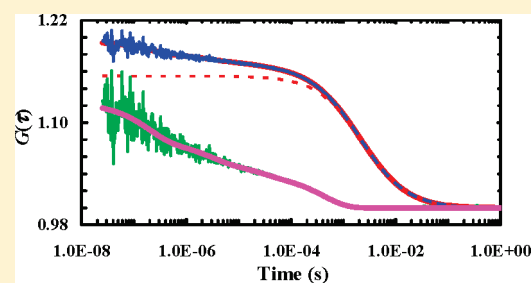
Photoinduced Electron Transfer and Fluorophore Motion as a Probe of the Conformational Dynamics of Membrane Proteins: Application to the Influenza A M2 Proton Channel

Julie M. G. Rogers,^{†,§} Alexei L. Polishchuk,^{†,§} Lin Guo,^{†,§} Jun Wang,[†] William F. DeGrado,^{†,‡} and Feng Gai^{*,†}

[†]Department of Biochemistry and Molecular Biophysics, School of Medicine, and [‡]Department of Chemistry, University of Pennsylvania, Philadelphia, Pennsylvania 19104, United States

Supporting Information

ABSTRACT: The structure and function of the influenza A M2 proton channel have been the subject of intensive investigations in recent years because of their critical role in the life cycle of the influenza virus. Using a truncated version of the M2 proton channel (i.e., M2TM) as a model, here we show that fluctuations in the fluorescence intensity of a dye reporter that arise from both fluorescence quenching via the mechanism of photoinduced electron transfer (PET) by an adjacent tryptophan (Trp) residue and local motions of the dye molecule can be used to probe the conformational dynamics of membrane proteins. Specifically, we find that the dynamics of the conformational transition between the N-terminal open and C-terminal open states of the M2TM channel occur on a timescale of about 500 μ s and that the binding of either amantadine or rimantadine does not inhibit the pH-induced structural equilibrium of the channel. These results are consistent with the direct occluding mechanism of inhibition which suggests that the antiviral drugs act by sterically occluding the channel pore.



INTRODUCTION

The M2 proton channel of the influenza A virus is composed of four relatively small (97 residues) monomers that span the viral envelope as a helical transmembrane bundle.¹ Among its several functions,^{2,3} M2 mediates the acidification of the viral interior from an acidic endosome lumen, which enables the release of viral RNA in a form competent for replication within the host cell.¹ Thus, it has been identified as a major target for anti-influenza drugs.⁴ Recently, it has been shown that the tetrameric assembly, proton translocation function, and inhibition of full-length M2 are maintained by a remarkably small, 25-residue peptide, M2TM.³ Because of its smaller size, the M2TM transmembrane helical bundle provides a unique model system for examining the structural and dynamic determinants of the M2 function.

Although the mechanism of proton translocation through M2 has been a subject of much debate,^{5,6} two amino acids within the transmembrane domain, His37 and Trp41, have been shown to be critical to M2 proton translocation, with His 37 mediating the proton selectivity and pH activation of transport^{7,8} and Trp41 being required to facilitate largely unidirectional proton flow across the membrane in an N-terminal to C-terminal fashion.⁹ Recently, several high-resolution structures of the M2 transmembrane bundle have been obtained,^{10–12} suggesting that the conformation of the tetrameric helical bundle changes significantly in response to a pH change as the bundle assumes a cylindrical shape at high pH (referred to as N-open hereafter), but a cone shape at low pH where the C-terminal ends of the transmembrane helices become further separated (referred to as C-open hereafter). This pH-induced conformational change and the

concerted rotamer shift of the Trp41 side chain, which interacts with His37 in a cation π -like fashion,¹³ are believed to be key determinants of the M2 proton translocation capability.¹⁴ It has been hypothesized that the mechanism is transporter-like, involving the protonation of His37 from the N-terminal side via an open N-terminal pore whereas the C-terminal pore exit is closed off by Trp41 side chains.¹⁴ After a conformational shift that closes off the N-terminal end of the bundle and opens the C-terminal end, His37 releases its proton to pore waters on the C-terminal side of the membrane.¹⁴ In this model, the opening/closing motions of the channel occur at all pH values, and a change in pH induces a shift in the equilibrium between N-open and C-open^{14,15} and possibly other stable intermediates.

Although this mechanistic hypothesis is supported by a recent molecular dynamics simulation,¹⁴ a direct experimental assessment of the underlying conformational transitions upon protonation of the M2 tetramer is still lacking. In addition, as a result of two conflicting high-resolution structures, the mechanism of inhibition by two extensively used anti-influenza agents, amantadine and rimantadine,¹⁶ is also under debate. One view is based on a crystal structure in which amantadine was found in the interior of the channel and suggests that the drug functions by occluding the channel pore.¹¹ The other view, which is based on an NMR structure in which the rimantadine binding site was outside the channel, suggests that conduction is prevented allosterically and that

Received: February 7, 2011

Revised: February 22, 2011

Published: March 14, 2011

drug binding stabilizes the N-open conformation.¹⁰ More recently, an NMR structure showed that amantadine is bound to the channel pore at stoichiometric concentrations and to the outside of the channel only when the concentration is increased.¹²

To provide further insight into the pH-induced structural changes of the M2 channel embedded in fully hydrated membranes, we use fluorescence correlation spectroscopy (FCS) in conjunction with photoinduced electron transfer (PET) to measure how the fluctuation dynamics of the Trp41 side chain in M2TM change as a function of pH. Via the mechanism of PET, Trp can effectively quench the fluorescence of a series of oxazine dye molecules, such as MR121 and Atto 655, when the indole ring and the dye of interest are brought sufficiently close to one another.^{17,18} Thus, the protein conformational dynamics involving motions that result in changes in the separation distance between Trp and the dye reporter could be probed via FCS because such motions would induce fluctuations in the fluorescence of the reporter. Herein, we introduce an Atto 655 dye at position 40 via a Cys mutant of M2TM, Leu40/Cys (the labeled peptide is hereafter referred to as Atto-40-M2TM), and use PET to probe the M2TM channel dynamics. In addition, we show that the dynamic motion of the dye molecule is also a useful probe of the dynamics and/or conformational equilibrium of the M2TM tetramer. Taken together, our results support the transporter-like mechanism^{14,15} and also the measurements indicating that drugs act by occluding the channel.^{11,12}

EXPERIMENTAL SECTION

Peptide Synthesis and Purification. Peptides were synthesized by solid-phase Fmoc synthesis as C-terminal amides, cleaved and purified as previously described.¹⁹ The WT M2TM peptide (22–46), (sequence SSDPLVVAASIIIGLHLILWILDRL), the M2TM W41F variant, was not N-terminally acetylated, and an N-terminal acetyl group was installed on the WT M2TM 19–46 peptide (M2TM 22–46 with an additional sequence of CND at the N terminus) and on the other Cys-containing peptides used in these experiments (M2TM L40C, M2TM L40C W41F, and M2TM I32C). Following RP-HPLC purification, peptides were lyophilized, the purity was assayed by analytical RP-HPLC, and the identity was confirmed by MALDI-TOF mass spectrometry.

Peptide Labeling. M2TM peptides were labeled with Atto 655 maleimide (Atto-Tec, Siegen, Germany or Sigma-Aldrich, St. Louis, MO). Labeling reactions were performed with an ~10–20-fold excess of dye to peptide. Peptide concentrations were quantified by UV–vis spectrophotometry in mixtures of acetonitrile and water that provided optimum solubility. An extinction coefficient of 5500 M⁻¹cm⁻¹ at 280 nm was used for Trp-containing peptides, and an extinction coefficient of 195 M⁻¹cm⁻¹ at 257 nm was used for W41F mutants. The purchased dye solid (1 mg) was dissolved in acetonitrile. Peptide and dye stock were added to an acetonitrile–water mixture with added sodium phosphate buffer at pH ~7.3. Total reaction mixture volumes were typically less than 0.5 mL. The reaction mixture was stirred at room temperature and monitored by reverse-phase analytical HPLC using gradients similar to those in preparative purification methods for M2TM peptides.¹⁹ Reactions were usually complete within 3 h, as evidenced by the absence of the starting material peak from the trace and the appearance of a new peak absorbing strongly at 630 nm and eluting near the time of the starting material peak. Upon completion, reaction mixtures were quenched with a drop of trifluoroacetic acid and diluted as necessary to facilitate handling. Owing to the small amount of sample, labeled peptides were purified using serial analytical HPLC injections of the reaction mixture. Labeled peptide fractions (eluting as a blue solution) were lyophilized and assayed for identity and purity by MALDI-TOF mass spectrometry.

M2TM Reconstitution into Small Unilamellar Vesicles.

Lipid films (2.5 μmol total lipid) of 4:1 POPC/POPG (Avanti Polar Lipids, Alabaster, AL) were prepared by co-drying chloroform stocks of the phospholipids under a stream of nitrogen or argon, followed by lyophilization and storage at -20 °C. Unlabeled peptide (6.25 nmol, 1:400 monomer/lipid) in 40 mM octylglucoside (<50 μL) was added dropwise to the lipid film, followed by 0.25 nmol (1:10 000 monomer/lipid) of labeled peptide (<10 μL). The W41F variant peptides (labeled and unlabeled) were added to the lipid film as ethanolic stocks because of limited solubility in octylglucoside; the mixture was vortex mixed and redried under a stream of inert gas. Extinction coefficients for unlabeled peptides were the same as those given above, whereas labeled peptides were quantified using the dye absorption maximum of 1.25 × 10⁵ M⁻¹cm⁻¹ near 660 nm, where the peptide components have no additional absorbance.

The sample mixture was buffered with 5 mM NaMOPS at pH 7 and 100 mM NaCl, and the volume increased to 500 μL with periodic vortex mixing. The mixture underwent 15 freeze–thaw cycles, and then the volume was increased to 1 mL. The sample was dialyzed overnight against 1 to 2 volumes of 1 L of 5 mM NaMOPS at pH 7 and 100 mM NaCl using 10 kDa cutoff Slide-A-Lyzer cassettes (Pierce, Rockford, IL), with Amberlite XAD-4 resin added to bind residual OG. Following dialysis, the sample was sonicated extensively on ice using a Fisherbrand model 500 sonic dismembrator (Fisher Scientific, Pittsburgh, PA), followed by centrifugation in a benchtop microcentrifuge to sediment sonicator tip shavings and any aggregates. The supernatant was isolated and maintained on ice prior to experiments, which were performed within 4 days of sample preparation.

FCS Sample Preparation. For M2 experiments, liposome samples were diluted 1:10 in buffers consisting of 80 mM NaCl and 25 mM NaMOPS (higher pH ranges) or NaOAc (lower pH ranges), depending on the desired pH. Some samples, as described in the text, contained either 100 μM amantadine or 20 μM rimantadine. Samples were placed on glass coverslips that had been modified with 2-[methoxy(polyethyleneoxy)propyl]-trimethoxysilane (Gelest, Morrisville, PA). After acid washing, glass coverslips were treated with a solution that was prepared as follows: the pH of a 95% ethanol, 5% water solution was adjusted to 5.3 with acetic acid, and 2% (by volume) 2-[methoxy(polyethyleneoxy)propyl]trimethoxysilane was then added and allowed to sit for 5 min (to allow hydrolysis). Coverslips were added to the solution for 2 min, removed and rinsed vigorously with ethanol, and then allowed to dry for 24 h. Coverslips were further rinsed with water and dried before use.

FCS Setup and Data Analysis. The details of the FCS setup have been described elsewhere.²⁰ In the current case, excitation of the Atto 655 dye was accomplished by the ~30 μW 630 nm line of a helium–neon laser (JDS Uniphase Corporation, Milpitas, CA). Each FCS curve was accumulated for a duration of 300 s, and an average of 10 to 30 such FCS curves was used in the subsequent data analysis. The FCS data were fit to the following equation (or other models discussed in the text)²¹

$$G(\tau) = \frac{1}{N} \left(\left(\frac{1}{1 + \frac{\tau}{\tau_D}} \right) \left(\frac{1}{1 + \frac{\tau}{\omega^2 \tau_D}} \right)^{1/2} \right) \times \left(\frac{1 - \sum_{i=1}^m \left(T_i - T_i \exp\left(-\frac{\tau}{\tau_i}\right) \right)}{1 - \sum_{i=1}^m T_i} \right) \quad (1)$$

where τ_D represents the 3-D diffusion time constant, ω refers to the axial–lateral-dimension ratio of the confocal volume element, N represents the number of fluorescent molecules in the confocal volume, and τ_i and T_i represent the respective time constant and amplitude of the dynamic

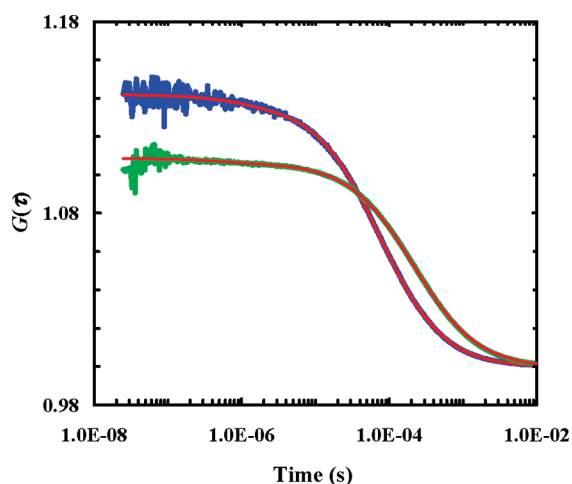


Figure 1. Representatives FCS curves obtained with the free dye, Atto 665, in buffer solution (blue) and Atto-40-M2TM in ethanol (green). The red lines represent the best fit of these data to eq 1 with $m = 1$ and the following parameters: $\tau_D = 73.6 \mu\text{s}$, $\tau_1 = 0.89 \mu\text{s}$, and $T_1 = 0.03$ for the free dye and $\tau_D = 214 \mu\text{s}$, $\tau_1 = 0.54 \mu\text{s}$, and $T_1 = 0.02$ for the peptide.

component i . The values of ω were determined by fitting the FCS data of the fluorescent ATTO 655 dyes in water.

RESULTS AND DISCUSSION

Atto 655 and Atto-40-M2TM in Solution. As shown (Figure 1), the FCS curve obtained with the free Atto 655 dye in water can be adequately fit by eq 1 with a diffusion time (τ_D) of $73.6 \mu\text{s}$ and a single dynamic component of $0.89 \mu\text{s}$ (amplitude = 0.03). Similarly, the FCS curve measured with Atto-40-M2TM in ethanol can also be well described by eq 1 with a τ_D of $214 \mu\text{s}$ and a single dynamic component of $0.54 \mu\text{s}$ (amplitude = 0.02) (Figure 1). We attribute this dynamic component to triplet-state formation because its relaxation time is within the timescale typical of the triplet lifetime of standard dyes.²² The small amplitude (0.02–0.03) of this component is also supportive of this assignment because it is known that Atto dyes have very low intersystem crossing yields.^{23,24} In the case of Atto-40-M2TM peptide, the lack of other dynamic components indicates that PET is not detectable in solution, suggesting that either an encounter complex between the Trp residue and the dye is never formed or the underlying PET dynamics are too slow/fast to be observed.²⁵

Liposome-Bound Atto-40-M2TM₄. To perturb the native properties of the M2TM channel minimally, the fluorescently labeled M2TM tetramers were assembled in the membrane of POPC/POPG (4:1) liposomes in a manner (see sample preparation) such that the large majority of tetramers contained either no or only one Atto-40-M2TM (such a tetramer is hereafter referred to as Atto-40-M2TM₄). In addition, it was estimated that only approximately 10% of the liposomes contained one Atto-40-M2TM₄ and that the concentration of Atto-40-M2TM₄ containing or fluorescent liposome was about 5 to 6 nM. As shown (Figure 2), the FCS curve obtained with Atto-40-M2TM₄ at pH 6.5 is quite different from that of the Atto-40-M2TM monomer in solution (Figure 1). In fact, we found that at least four dynamic components were required to yield a satisfactory fit of these FCS data using eq 1 and a diffusion time of $2359 \pm 150 \mu\text{s}$. As shown in the Supporting Information (Figure S1), fitting these data to a simpler model yields an unsatisfactory fit. As indicated (Figure 2), these dynamic components are well separated in

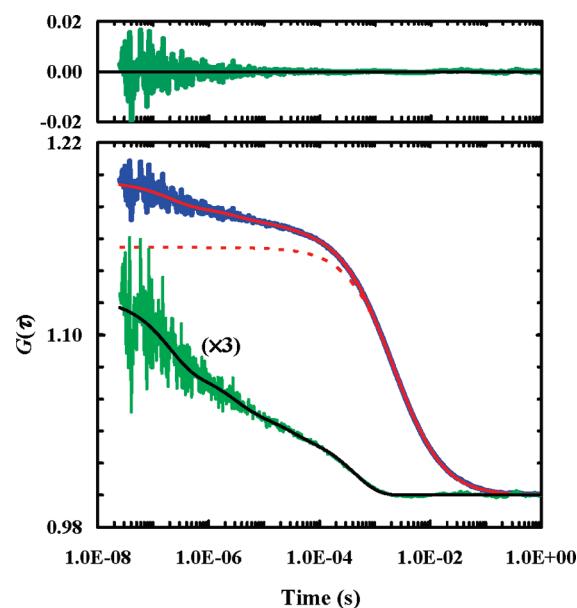


Figure 2. Representatives FCS curve (blue) obtained with Atto-40-M2TM₄ at pH 6.5. The solid red line represents the best fit of these data to eq 1 with $m = 4$. The dashed red line represents the diffusion component, the green line represents the nondiffusional portion of the FCS curve (i.e., $G(\tau) - \text{diffusion component}$), and the black line corresponds to the difference between the solid red line and the dashed red line. Also shown in the top panel are residuals of the fit.

time and have the following respective time constants: 0.189 ± 0.050 , 2.66 ± 0.50 , 24.0 ± 4.0 , and $508 \pm 80 \mu\text{s}$. The $2.7 \mu\text{s}$ component most likely arises from triplet formation because the free dye exhibits a similar dynamic component and its amplitude shows a dependence on the laser power (Figure S2 in Supporting Information). Moreover, results obtained from a control FCS experiment (Figure S3 in Supporting Information) indicated that those longer dynamic components are not due to the variability in the size of the liposome.

A simple estimate of the rotational diffusion coefficient of the liposome using the Einstein–Smoluchowski relation and the hydrodynamic radius of the liposome, which was determined on the basis of its translational diffusion time (i.e., $\tau_D = 2400 \mu\text{s}$), indicates that the liposome should rotate on a timescale of $\sim 17 \mu\text{s}$. Thus, we attribute the $24.8 \pm 4.0 \mu\text{s}$ component to the rotational motion of the liposome. Although either one or both of the remaining dynamic components could be attributed to PET, further experiments are required to determine their origin(s). Therefore, we performed control FCS experiments using a fluorescently labeled but Trp-free double mutant of M2TM (i.e., Leu40/Cys/Trp41/Phe) with the Atto 655 dye introduced at the Cys position. (The resultant peptide is hereafter referred to as Atto-Phe-M2TM.) Previous studies have shown that the Trp41/Phe mutant of M2TM exists in a tetrameric form in the POPC/POPG (4:1) membranes and conducts but lacks rectifying behavior.²⁶ In addition, the Trp-to-Phe mutation should eliminate PET because Trp41 is the only residue in M2TM that can quench the fluorescence of Atto 655.¹⁸ Similar to the Atto-40-M2TM₄ liposome samples, the Atto-Phe-M2TM-containing tetramers (referred to hereafter as Atto-Phe-M2TM₄) were prepared so that each tetramer contains only one Atto-Phe-M2TM. As shown (Figure 3), the FCS curves obtained with Atto-Phe-M2TM₄ at different pH values can be well described by eq 1 with $\tau_D = 2192 \mu\text{s}$ and only three dynamic components, with time constants at $10 \pm 2 \mu\text{s}$ (due to liposome rotation), $1.0 \pm 0.2 \mu\text{s}$ (due to the triplet

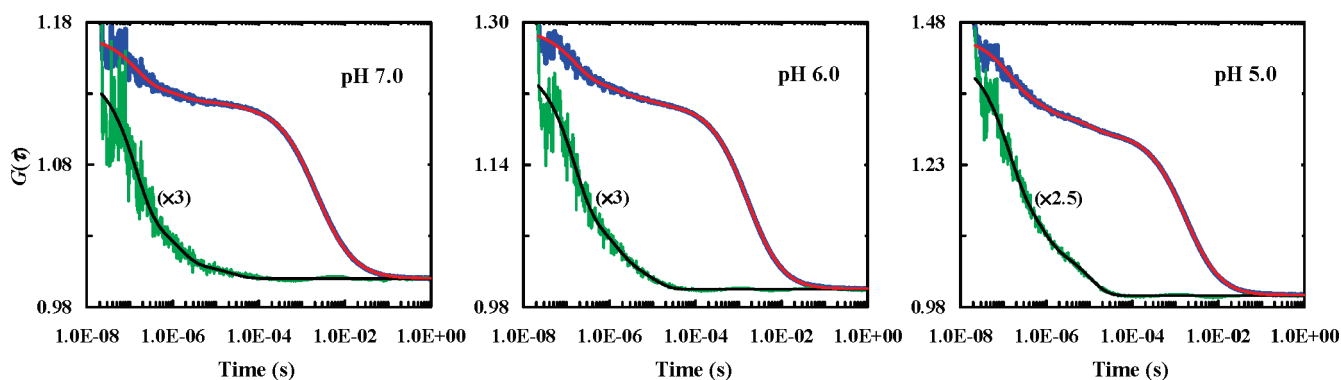


Figure 3. Representative FCS curves obtained with Atto-Phe-M2TM₄ at different pH values, as indicated. The red line represents the best fits of the FCS data to eq 1 with $m = 3$. The green line represents the nondiffusional portion of each FCS curve (i.e., $G(\tau)$ – diffusion component), and the black line corresponds to its fit (i.e., fit of $G(\tau)$ – diffusion component).

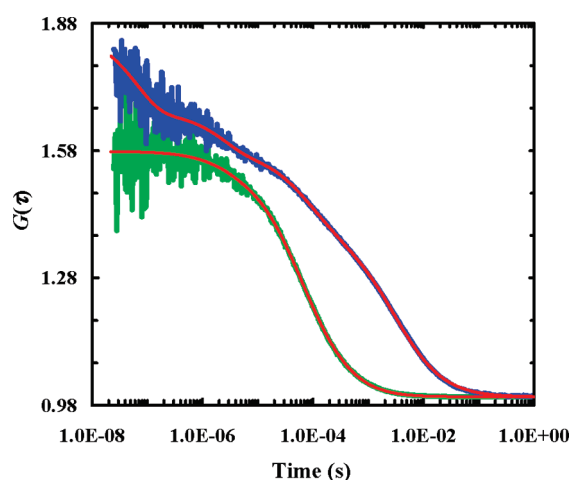


Figure 4. Representative FCS curves obtained with pHLIP in the presence (blue) and absence (green) of membranes at pH 4.

state), and $0.15 \pm 0.03 \mu\text{s}$. Thus, the absence of the $508 \mu\text{s}$ component, which was observed in the experiments with Atto-40-M2TM₄, indicates that this component is associated with PET. However, it is clear that the Trp-to-Phe mutation does not eliminate the nanosecond component, indicating that it has a different origin.

We attribute this nanosecond FCS component to internal fluctuations of the fluorescent reporter, either because of the rotation of the dye or the local dynamics of the backbone. Because the excitation light in the current case is linearly polarized, such motions would result in changes in the direction of the absorption transition dipole of the fluorophore and hence fluctuations in its fluorescence intensity. Of course, only those motions that are sufficiently slow are amenable to FCS detection.^{27,28} To verify this point, we recorded the FCS curves of a fluorescently labeled pH low-insertion peptide (pHLIP)²⁹ in solution and membrane environments. The pHLIP peptide (the sequence used in the current study is ACEQNPIYWARYAD-WLFTTPLLDDLALLVDADEGTG) is designed to form a monomeric transmembrane α -helix at acidic pH.²⁹ In the current case, the fluorescence reporter (tetramethylrhodamine) is appended to the N terminus of the peptide through the Cys residue. As shown (Figure 4), in solution the dynamics of the peptide and the dye are too fast to be measured by our FCS setup; however, when bound to POPC membranes as a transmembrane α -helix at pH 4,³⁰ a component of $0.064 \pm 0.030 \mu\text{s}$ is readily detectable. Taken together,

these results support the notion that the local fluctuation dynamics of a dye reporter can be measured via FCS by using linearly polarized excitation light.

Liposome-Bound Atto-40-M2TM₄ at Different pH Values.

Previous studies have suggested that the M2 channel undergoes a significant change in its structural equilibrium in response to a pH change from 7.0 to 5.0.^{10,11} Thus, we performed a series of FCS measurements using Atto-40-M2TM₄ in the pH range of 5.0–7.5. As shown (Figure 5), the resultant FCS curves, especially the nanosecond component, show a clear dependence on pH although the FCS signals are dominated by the diffusion component. To determine the amplitudes of the local fluctuation and the PET components better, we globally fit the FCS curves obtained at different pH values to the following model

$$G(\tau, \text{pH}) = \frac{1}{N_{\text{pH}}} \left(\left(\frac{1}{1 + \frac{\tau}{\tau_{\text{D}}}} \right) \left(\frac{1}{1 + \frac{\tau}{\omega^2 \tau_{\text{D}}}} \right)^{1/2} \right) \times \left(1 + A_{\text{R,pH}} \exp \left(-\frac{\tau}{\alpha (\tau_{\text{D}})^3} \right) \right) \times \left(\frac{1 - \sum_{i=1}^m \left(T_{i,\text{pH}} - T_{i,\text{pH}} \exp \left(-\frac{\tau}{\tau_i} \right) \right)}{1 - \sum_{i=1}^m T_{i,\text{pH}}} \right) \quad (2)$$

where the overall or global rotational time (τ_{R}) of the liposome, whose amplitude is $A_{\text{R,pH}}$ is assumed to be proportional to the third power of its translational diffusion time (τ_{D}).^{31,32} The three exponentials that were needed in the last term include those assigned to the triplet state, local fluctuation, and PET components. Although N_{pH} , $T_{i,\text{pH}}$, and $A_{\text{R,pH}}$ were allowed to vary locally, all other parameters, including τ_{D} , τ_i and α , were globally restrained across all pH values during the fitting. As shown (Figure 5 and Figure S4 in the Supporting Information), this model fits the FCS curves well. Because the triplet-state dynamics of Atto 655 and the translational and rotational diffusion of the liposome do not provide any information regarding the dynamics of the channel, in the following discussion we focus on the PET component ($\tau = 673 \pm 80 \mu\text{s}$) and the local fluctuation component ($\tau = 0.20 \pm 0.04 \mu\text{s}$).

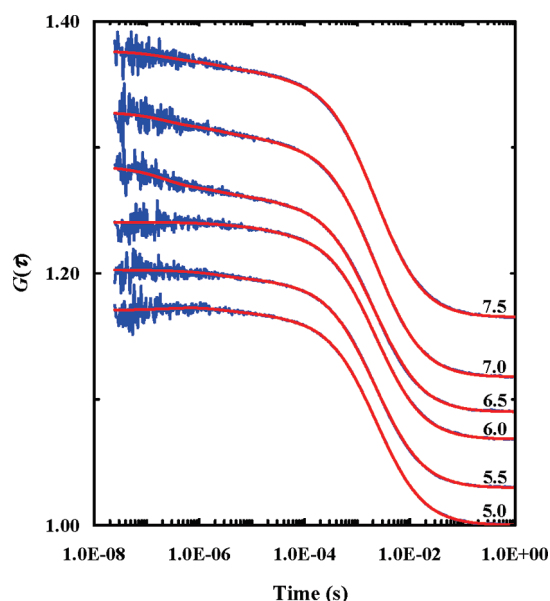


Figure 5. Representative FCS curves (blue) obtained with Atto-40-M2TM₄ at different pH values, as indicated. These data have been offset for clarity. Red lines represent the global fits of these data to eq 2 with $m = 3$. The fitting parameters and residuals of the fit are given in the Supporting Information (Table S1 and Figure S5).

PET Component. PET has been used to report peptide dynamics from nanosecond to millisecond timescales.^{25,33} In our case, PET yields a relaxation time of 673 μ s whose amplitude exhibits a gradual decrease with decreasing pH (Figure 6). The latter is consistent with the notion that the M2 channel exists in at least two conformational states.^{14,15} The amplitude of the PET component represents the percentage of the peptide that is in the fluorescent dark state because of the PET interaction. In the current study, the fluorescent dark state induced by PET corresponds to the N-open state. At high pH (e.g., pH 7 and above), the N-open state in which the C-terminal regions of the four peptides are in closest proximity^{10,11} is stabilized, yielding the largest PET. However, at low pH (e.g., pH 5) the C-open state is preferred, where the Trp41 moves away from position 40 because of the protonation of His37 residues that causes a rotamer flip of the Trp residues.¹¹ The rate of the PET component is comparable to the turnover rate (~ 1000 protons/s) of the M2 channel measured at low pH.³⁴ Thus, it is possible that this component reports the actual opening/closing of the M2TM channel. This idea is corroborated by recent simulations that suggest that the opening/closing motions of the channel occur at all pH values.^{14,15}

Local Fluctuation Component. The amplitude of the internal fluctuation component shows a drastic decrease between pH 6.5 and 6.0 (Figure 6), a pH range that has been shown to activate the M2 channel.³⁴ Thus, this coincidence suggests that this FCS component is a useful probe of the conformational equilibrium of the M2TM channel. In particular, this component exhibits a relatively large amplitude when the M2TM tetramer favors the N-open state at high pH, whereas it practically disappears when the C-open state is favored at low pH. It appears from a fitting of the intensities to a two-state model that this transition is consistent with a published pK_a value (6.3) of the histidine residue.³⁵

There are two possible reasons that could lead to the disappearance of this component at low pH. The first possibility is that the dye fluctuates too quickly (faster than 40 ns) to be resolved by our FCS

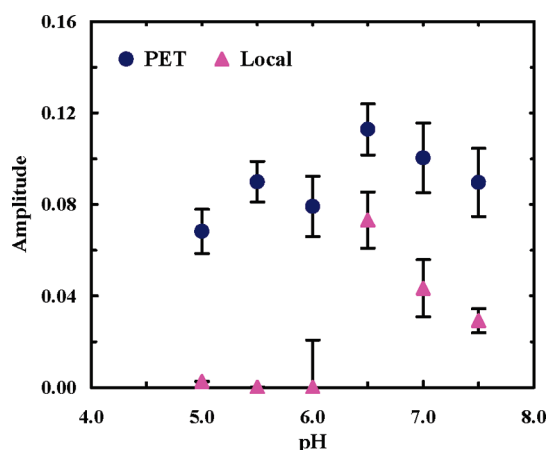


Figure 6. Amplitudes of the PET and local dynamic components of Atto-40-M2TM₄ versus pH. Errors were estimated from multiple measurements.

setup when the channel is in its C-open state. In support of this, previous studies have shown that at low pH the backbone of M2TM becomes more dynamic^{10,36} and that Leu40 is less restricted by other chains in the tetramer and is also more accessible to the interior of the channel.¹¹ The other possibility is that the motion of the dye becomes too restricted to induce any measurable fluctuations in its fluorescence. To understand the origin of the pH dependence of this local component better, we performed further control FCS experiments using a different fluorescently labeled M2TM peptide, with the Atto 655 dye introduced at position 32 using the Ile32/Cys mutant. (The M2TM tetramer containing this peptide is hereafter referred to as Atto-32-M2TM₄.) Because Ile32 is close to the middle of the channel with its side chain facing the lipids, it is expected that the local fluctuation component of Atto-32-M2TM₄ will be less sensitive to pH. In addition, it is expected that the PET component will disappear because in this case the Trp residues are too far from the dye to show any appreciable fluorescence quenching. As shown (Figure 7), the FCS curves obtained with Atto-32-M2TM₄ indeed lack the PET component, but the local dynamic component is present over the entire pH range studied. Taken together, these data further illustrate that this dynamic component is sensitive to the local environment and that when the dye reporter is placed at an appropriate position it can be used as a valuable probe of the M2TM tetramer conformational equilibrium and dynamics.³⁷ This statement is further corroborated by the Atto-Phe-M2TM₄ results, which show that this FCS component is present over the entire pH range studied, suggesting that the deletion of the key His-Trp interactions²⁶ makes the tetramer adopt a conformation that is similar to the closed state or a cylindrically shaped structure of the M2TM channel.¹¹

Effect of Amantadine. The above results suggest that the 0.2 μ s component observed with Atto-40-M2TM₄ is a useful probe of the pH-induced conformational shift of the M2TM tetramer between the N-open and C-open states. Thus, in the following experiments we use it to probe how drug binding affects the conformational equilibrium of the M2TM channel. As shown (Figure 8), the binding of amantadine to Atto-40-M2TM₄ does not significantly change the FCS curves. Similar to that observed for drug-free Atto-40-M2TM₄, the amplitude of the PET component ($\tau = 557 \pm 80 \mu$ s) shows a minor decrease with decreasing pH from 7.5 to 5.0 and the amplitude of the local fluctuation component ($0.16 \pm 0.04 \mu$ s) exhibits a large decrease

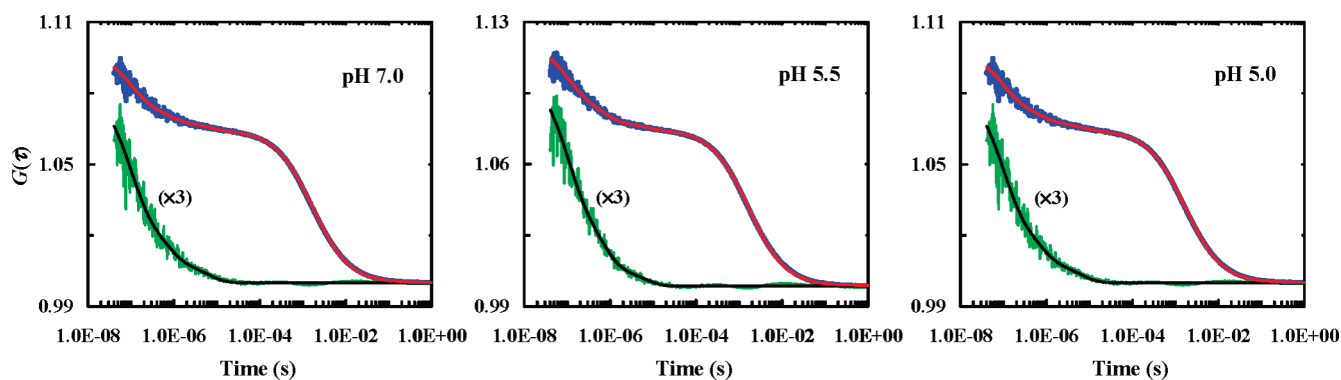


Figure 7. Representative FCS curves obtained with Atto-32-M2TM₄ at different pH values, as indicated. Red lines represent the global fits of these data to eq 2 with $m = 2$, $\tau_1 = 0.092 \mu\text{s}$ (with $T_1 = 0.16, 0.20$, and 0.21 for pH 7.0, 5.5, and 5.0, respectively), and $\tau_2 = 0.57 \mu\text{s}$ (with $T_2 = 0.10, 0.13$, and 0.09 for pH 7.0, 5.5, and 5.0, respectively). The green line represents the nondiffusional portion of each FCS curve (i.e., $G(\tau) - \text{diffusion component}$), and the black line corresponds to its fit (i.e., fit of $G(\tau) - \text{diffusion component}$). The residuals of the fit are given in the Supporting Information (Figure S4).

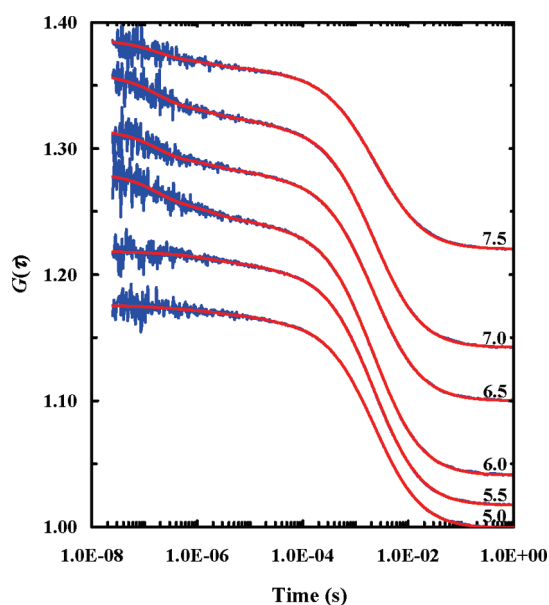


Figure 8. Representative FCS curves obtained with drug-bound Atto-40-M2TM₄ at different pH values, as indicated. These data have been offset for clarity. Red lines represent the global fits of these data to eq 2 with $m = 3$. The fitting parameters and residuals are given in the Supporting Information (Table S2 and Figure S6).

between pH 6.0 and 5.0 (Figure 9). The increase in the rate of the PET process upon drug binding is consistent with the notion that the drug will affect the His-Trp interactions and thus the Trp dynamics. However, taken together, these results suggest that drug binding does not prevent the M2TM tetramer from undergoing the underlying shift in conformational equilibrium upon protonation of the His residues, although according to the fit the transition seems to occur at a lower pH, which is expected given that the pK_a of the His residues shifts to 5.4 in the presence of amantadine.³⁸ In other words, these results are consistent with the crystal structure of Stouffer et al., which shows that amantadine binds to the center of the M2TM channel and, as a result, physically occludes the pore but does not inhibit the pH-appropriate conformational equilibrium shift of the channel.^{11,12} The results obtained with another drug, rimantadine (data not shown), also corroborate this conclusion.

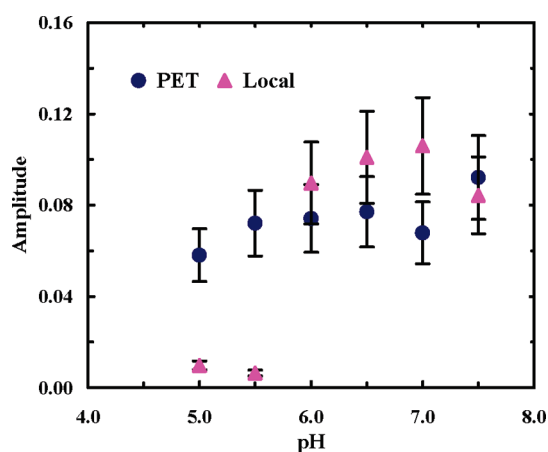


Figure 9. Amplitudes of the PET and local dynamic components obtained with drug-bound Atto-40-M2TM₄ vs pH, as indicated.

CONCLUSIONS

We employ fluorescence correlation spectroscopy (FCS) to investigate the conformation and conformational dynamics of a truncated version of the influenza A M2 proton channel, M2TM, in the pH range of 5.0–7.0 with and without the presence of inhibition drugs. Our results show that both the photoinduced electron transfer (PET) process from Trp to the dye reporter and the local fluctuation motions of the dye can be used to probe changes in the structure and/or dynamics of the membrane-bound M2TM tetramer. In particular, our data support a proposed inhibition mechanism that involves the drugs binding to the interior of the channel and physically occluding the pore.

ASSOCIATED CONTENT

S Supporting Information. Control experiments, residual plots, and fitting parameters. This material is available free of charge via the Internet at <http://pubs.acs.org>.

AUTHOR INFORMATION

Corresponding Author

*E-mail: gai@sas.upenn.edu

Author Contributions

⁵These authors contributed equally to this work.

ACKNOWLEDGMENT

We gratefully acknowledge financial support from the National Institutes of Health (GM-065978) and the National Science Foundation (DMR05-20020).

REFERENCES

- (1) Pinto, L.; Lamb, R. *J. Biol. Chem.* **2006**, *281*, 8997.
- (2) Chen, B.; Leser, G. P.; Jackson, D.; Lamb, R. A. *J. Virol.* **2008**, *82*, 10059.
- (3) Ma, C.; Polishchuk, A. L.; Ohigashi, Y.; Stouffer, A. L.; Schön, A.; Magavern, E.; Jing, X.; Lear, J. D.; Freire, E.; Lamb, R. A.; DeGrado, W. F.; Pinto, L. H. *Proc. Natl. Acad. Sci. U.S.A.* **2009**, *106*, 12283.
- (4) Hay, A. J.; Wolstenholme, A. J.; Skehel, J. J.; Smith, M. H. *EMBO J.* **1985**, *4*, 3021.
- (5) Sansom, M. S. P.; Kerr, I. D.; Smith, G. R.; Son, H. S. *Virology* **1997**, *233*, 163.
- (6) Pinto, L. H.; Dieckmann, G. R.; Gandhi, C. S.; Papworth, C. G.; Braman, J.; Shaughnessy, M. A.; Lear, J. D.; Lamb, R. A.; DeGrado, W. F. *Proc. Natl. Acad. Sci. U.S.A.* **1997**, *94*, 11301.
- (7) Wang, C.; Lamb, R. A.; Pinto, L. H. *Biophys. J.* **1995**, *69*, 1363.
- (8) Venkataraman, P.; Lamb, R. A.; Pinto, L. H. *J. Biol. Chem.* **2005**, *280*, 21463.
- (9) Tang, Y. J.; Zaitseva, F.; Lamb, R. A.; Pinto, L. H. *J. Biol. Chem.* **2002**, *277*, 39880.
- (10) Schnell, J.; Chou, J. *Nature* **2008**, *451*, 591.
- (11) Stouffer, A. L.; Acharya, R.; Salom, D.; Levine, A. S.; Di Costanzo, L.; Soto, C. S.; Tereshko, V.; Nanda, V.; Staybrook, S.; DeGrado, W. F. *Nature* **2008**, *451*, 596.
- (12) Cady, S. D.; Schmidt-Rohr, K.; Wang, J.; Soto, C. S.; DeGrado, W. F.; Hong, M. *Nature* **2010**, *463*, 689.
- (13) Okada, A.; Miura, T.; Takeuchi, H. *Biochemistry* **2001**, *40*, 6053.
- (14) Khurana, E.; Dal Peraro, M.; DeVane, R.; Vemparala, S.; DeGrado, W. F.; Klein, M. L. *Proc. Natl. Acad. Sci. U.S.A.* **2009**, *106*, 1069.
- (15) Yi, M.; Cross, T. A.; Zhou, H. X. *Proc. Natl. Acad. Sci. U.S.A.* **2009**, *106*, 13311.
- (16) Davies, W. L.; Grunert, R. R.; Haff, R. F.; McGahen, J. W.; Neumayer, E. M.; Paulshock, M.; Watts, J. C.; Wood, T. R.; Hermann, E. C.; Hoffmann, C. E. *Science* **1964**, *144*, 862.
- (17) Doose, S.; Neuweiler, H.; Sauer, M. *ChemPhysChem* **2005**, *6*, 2277.
- (18) Marmé, N.; Knemeyer, J.-P.; Sauer, M.; Wolfrum, J. *Bioconjugate Chem.* **2003**, *14*, 1133.
- (19) Stouffer, A. L.; Nanda, V.; Lear, J. D.; DeGrado, W. F. *J. Mol. Biol.* **2005**, *347*, 169.
- (20) Guo, L.; Chowdhury, P.; Glasscock, J. M.; Gai, F. *J. Mol. Biol.* **2008**, *384*, 1029.
- (21) Aragòn, S. R.; Pecora, R. *J. Chem. Phys.* **1976**, *64*, 1791.
- (22) Van de Linde, S.; Kasper, R.; Heilemann, M.; Sauer, M. *Appl. Phys. B: Lasers Opt.* **2008**, *93*, 725.
- (23) Buschmann, V.; Weston, K. D.; Sauer, M. *Bioconjugate Chem.* **2003**, *14*, 195.
- (24) Dertinger, T.; Gregor, I.; Von Hocht, I. D.; Erdmann, R.; Krämer, B.; Koberling, F.; Hartmann, R.; Enderlein, J. *Prog. Biomed. Opt. Imaging Proc. SPIE* **2006**, *6092*, 609203.
- (25) Doose, S.; Neuweiler, H.; Barsch, H.; Sauer, M. *Proc. Natl. Acad. Sci. U.S.A.* **2007**, *104*, 17400.
- (26) Tang, Y.; Zaitseva, F.; Lamb, R. A.; Pinto, L. H. *J. Biol. Chem.* **2002**, *277*, 39880.
- (27) Borst, J. W.; Laptinok, S. P.; Westphal, A. H.; Kuhnemuth, R.; Hornen, H.; Visser, N. V.; Kalinin, S.; Aker, J.; van Hoek, A.; Seidel, C. A. M.; Visser, A. J. W. G. *Biophys. J.* **2008**, *95*, 5399.
- (28) Wei, C. Y. J.; Lu, C. Y.; Kim, Y. H.; Bout, D. A. V. *J. Fluoresc.* **2007**, *17*, 797.
- (29) Reshetnyak, Y. K.; Segala, M.; Andreev, O. A.; Engelman, D. M. *Biophys. J.* **2007**, *93*, 2363.
- (30) Guo, L.; Gai, F. *Biophys. J.* **2010**, *98*, 2914.
- (31) Tsay, J. M.; Doose, S.; Weiss, S. *J. Am. Chem. Soc.* **2006**, *128*, 1639.
- (32) Aizenbud, B. M.; Oppenheim, I. *Physica A* **1982**, *110*, 171.
- (33) Doose, S.; Neuweiler, H.; Sauer, M. *ChemPhysChem* **2009**, *10*, 1389.
- (34) Decoursey, T. E. *Physiol. Rev.* **2003**, *83*, 475.
- (35) Hu, J.; Fu, R.; Nishimura, K.; Zhang, L.; Zhou, H. X.; Busath, D. D.; Vijayvergiya, V.; Cross, T. A. *Proc. Natl. Acad. Sci. U.S.A.* **2006**, *103*, 6865.
- (36) Li, C.; Qin, H.; Gao, F. P.; Cross, T. A. *Biochim. Biophys. Acta, Biomembr.* **2007**, *1768*, 3162.
- (37) Sharma, M.; Yi, M.; Dong, H.; Qin, H.; Peterson, E.; Busath, D. D.; Zhou, H. X.; Cross, T. A. *Science* **2010**, *330*, 509.
- (38) Hu, J.; Fu, R.; Cross, T. A. *Biophys. J.* **2007**, *93*, 276.